Applied Physics
Express

The Japan Society of Applied Physics

LETTER • OPEN ACCESS

Kirigami-structured flexible heat flux sensor driven by the anomalous Nernst effect

To cite this article: Shusaku Saito *et al* 2026 *Appl. Phys. Express* **19** 053001

OPEN ACCESS
Applied Physics Express 19, 053001 (2026) LETTER
https://doi.org/10.35848/1882-0786/ae62c7

Kirigami-structured flexible heat flux sensor driven by the anomalous Nernst effect

Shusaku Saito[1,2], Takamasa Hirai[2*], Weinan Zhou[2], Shunsuke Mori[1,2], Kota Hasegawa[3], Rajkumar Modak[1,2], Fuyuki Ando[2], Yuya Sakuraba[2], and Ken-ichi Uchida[1,2]

[1]Department of Advanced Materials Science, Graduate School of Frontier Sciences, The University of Tokyo, Kashiwa 277-8561, Japan
[2]Research Center for Magnetic and Spintronic Materials, National Institute for Materials Science, Tsukuba 305-0047, Japan
[3]Resonac Corporation, Tsukuba 300-4247, Japan

*E-mail: HIRAI.Takamasa@nims.go.jp

Received March 25, 2026; revised April 15, 2026; accepted April 20, 2026; published online May 7, 2026

This letter proposes and demonstrates a flexible architecture for an anomalous-Nernst-effect-based heat flux sensor inspired by kirigami, a traditional Japanese paper-cutting art. A prototype device comprises an amorphous $Sm_{19}Co_{81}$ film and Ta/Au electrode on a flexible substrate pre-patterned with a periodic-cutting kirigami structure. The estimated heat flux sensitivity of the kirigami-structured sensor was comparable to that of a conventional sensor without a kirigami structure and remained unchanged even when it was stretched by 10%. Our approach opens a pathway toward versatile and mechanically compliant heat flux sensing that is applicable to various surfaces.

Heat flux sensing is an essential thermal management technology for understanding and controlling thermal transport in a wide range of systems, from electronic devices to materials processing and industry. Although various principles have been proposed for heat flux sensing, Seebeck-effect-based sensors are the most widely utilized. In the Seebeck effect, an electric field is generated in a direction parallel to a temperature gradient applied to a conductor. As a consequence, Seebeck-effect-based heat flux sensors adopt a structure consisting of a three-dimensional matrix of interconnected thermocouples with many junctions and electrodes, which can impose certain constraints on device durability, as these interfaces tend to be the primary points of failure. Because of the parallel relationship between the electric field and temperature gradient, such sensors inherently involve a trade-off; increasing the device thickness to enhance the output voltage simultaneously increases the thermal resistance along the heat-flow direction, where the presence of other multiple thickness components, including the substrate, electrodes, and junctions, also causes a high thermal resistance unavoidable, thereby leading to significant sensing errors.

Recently, heat flux sensors based on the anomalous Nernst effect (ANE) in conductive magnetic thin films have been proposed to overcome such issues.[1–9] ANE is one of the transverse magneto-thermoelectric effects and can generate an electric field in the direction of the cross product of an applied temperature gradient and magnetization. Owing to the orthogonal relationship between the electric field and temperature gradient in ANE, the output voltage can be proportionally enhanced by elongating the in-plane length of magnetic wires without increasing their thickness. Consequently, the basic module architecture of ANE-based heat flux sensors follows the configuration illustrated in Fig. 1(a). Here, magnetic and non-magnetic thin-film stripes are laterally and alternately connected on a substrate. Note that the non-magnetic wire is not essential; it can be replaced by a second magnetic material exhibiting the opposite sign of the anomalous Nernst coefficient,[8,10] or even by the same magnetic material provided that adjacent wires are magnetized in opposite directions.[11,12] When a flexible organic substrate is employed, the mechanical flexibility and durability of thin-film devices fabricated on it can be enhanced,[13–18] with maintaining the low thermal resistance. However, even with flexible substrates, it is often difficult to mount the sensors on arbitrarily curved surfaces; although ANE-based heat flux sensors on flexible substrates can be easily attached to a cylindrical heat source, their adhesion to a heat source with non-ruled curvature deteriorates due to the inherent tension of flexible substrates.[19–21]

In this study, we propose an advanced flexible architecture of ANE-based heat flux sensors by introducing the idea of kirigami. Kirigami is a traditional Japanese paper-cutting art, but has recently attracted attention in biotechnology and flexible electronics.[19–30] Applying a periodic-cutting pattern can make solid sheets greatly stretchable and flexible, improving three-dimensional deformation and adhesion on non-ruled surfaces.[20,24,27] As shown in Fig. 1(b), a kirigami structure should be applicable to the ANE-based heat flux sensor by cutting gaps between a magnetic and non-magnetic thin-film stripes [Fig. 1(c)]. Thus, here, we fabricated a prototype device of the ANE-based heat flux sensor with and without a periodic-cutting kirigami pattern and estimated the heat flux sensitivity, an indicator for the performance of heat flux sensors. The heat flux sensitivity remained unchanged after patterning kirigami and was further confirmed to be unaffected even under stretching enabled by kirigami structuring. Kirigami structuring is expected to substantially enhance the functionality and versatility of the ANE-based heat flux sensors, enabling adaptable heat flux sensing on non-ruled surfaces [Fig. 1(d)].

As the magnetic material for the ANE-based heat flux sensors, we selected an amorphous Sm-Co alloy film. Recently, it has been shown that Sm-Co-based alloy films exhibit large in-plane remanent magnetization and coercivity,[5] enabling zero-field operation of transverse thermoelectric generation. The film with a thickness of 100 nm was prepared on a 50-μm-thick UPILEX® (Ube

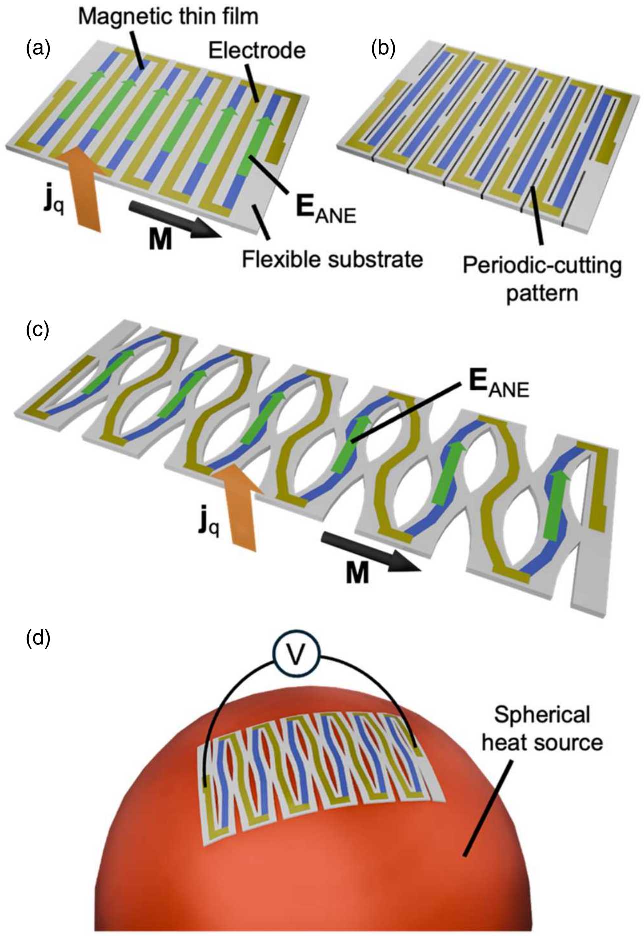

Fig. 1. (a)–(d) Schematics of a conventional ANE-based heat flux sensor without a kirigami structure (a), kirigami-structured heat flux sensor (b), kirigami-structured heat flux sensor under stretching (c), and kirigami-structured heat flux sensor attached on a spherical heat source (d). Here, $\mathbf{j}_q$, $\mathbf{M}$, and $\mathbf{E}_{ANE}$ denote the vectors of the heat flux density, magnetization, and electric field induced by ANE, respectively.

Corp.) via a layer-by-layer-design growth by magnetron sputtering using Sm and Co targets, where the deposition of 0.39-nm-thick Sm and 0.61-nm-thick Co layers was repeated 100 times [Fig. 2(a)]. Note that UPILEX® is a polyimide sheet known for its high temperature and mechanical durability and good surface smoothness, which is often used for flexible electronics.[31,32] A dc power source with 10 W for the Sm deposition and rf power source with 100 W for the Co deposition were used. A base pressure was $<6.0 \times 10^{-6}$ Pa and a process Ar gas pressure was 0.4 Pa. The structural and stoichiometric determination of the Sm-Co film deposited on the UPILEX® substrate was investigated using a scanning transmission electron microscope (STEM) with energy-dispersive X-ray spectroscopy (EDS) (Titan G2 80–200, FEI). In STEM experiments, the film was coated by Pt to protect the film surface from irradiation of a focused ion beam. As shown in Fig. 2(b), the halo rings observed in the electron diffraction pattern confirm the amorphous nature of the Sm-Co film and the cross-sectional high-angle annular dark field STEM image reveals the smooth interface and surface of the film even on the flexible organic substrate. Figures 2(c) and 2(d) represent the EDS elemental maps of Sm and Co, respectively. Uniform distribution of Sm and Co indicates that the Sm and Co

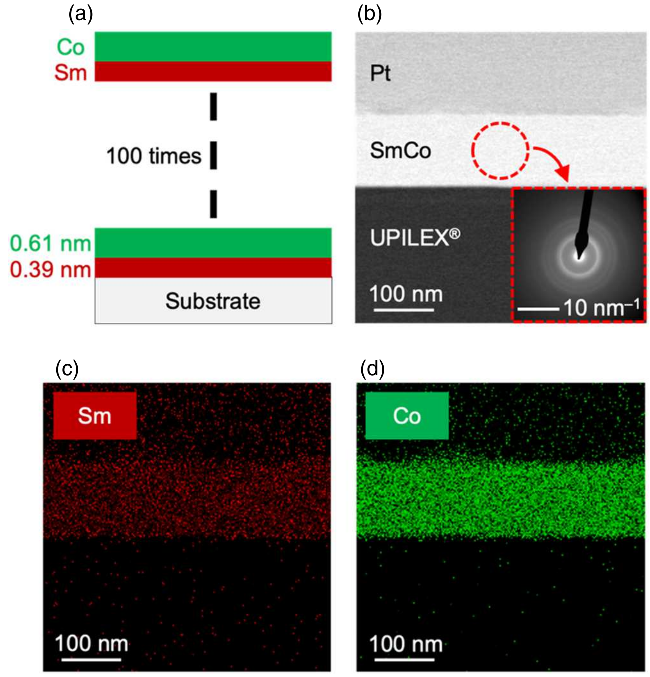

Fig. 2. (a) Schematic of the Sm-Co film prepared by the layer-by-layer-design growth. (b) Cross-sectional high-angle annular dark field STEM image of the Sm-Co film on a UPILEX® substrate. The inset selected area electron diffraction pattern was captured from the Sm-Co layer enclosed by the red-dashed circle. (c), (d) STEM-EDS elemental maps of Sm (c) and Co (d).

atoms were mixed as a solid solution or binary alloy although the Sm-Co film was deposited by the layer-by-layer-design growth. The EDS analysis also shows that the compositions of Sm and Co were 19.4 and 80.6 at%, respectively (thus, hereafter referred to as $Sm_{19}Co_{81}$), which is quite close to the $Sm_{20}Co_{80}$ composition reported to maximize the anomalous Nernst coefficient S_{ANE} for the amorphous Sm-Co film.[5]

Next, we investigated the thermoelectric and magnetic properties of the $Sm_{19}Co_{81}$ film. These measurements were done using the film on a sapphire *c*-plane substrate deposited simultaneously with that on the UPILEX® substrate. Our previous study has shown that, owing to the amorphous nature, the Sm-Co films maintain the same magneto-thermoelectric transport properties regardless of substrates.[5] The $Sm_{19}Co_{81}$ film was processed to a bar-shaped wire with a width of 3 mm and a length of 6 mm for measurements of ANE using photolithography and Ar ion milling, and then Ta/Au electrode pads were formed by the lift-off method. Figure 3(a) shows the result of the ANE measurement of the $Sm_{19}Co_{81}$ film at room temperature. In this measurement, the temperature gradient ∇T and external magnetic field H were applied in the film width and thickness directions, respectively. The ∇T value was quantified using an infrared camera by coating the film surface with black ink before sweeping H and the transverse thermoelectric voltage V_T was measured at various ∇T values.[33,34] The V_T signal showing the odd dependence on H was observed, with the V_T value saturating for $|\mu_0 H| > 2.5$ T, with μ_0 being the vacuum permeability, and increasing monotonically with increasing the ∇T value, whose behavior was totally consistent with the transverse thermoelectric generation due to ANE. The electric field induced by ANE, E_{ANE}, was calculated by dividing the

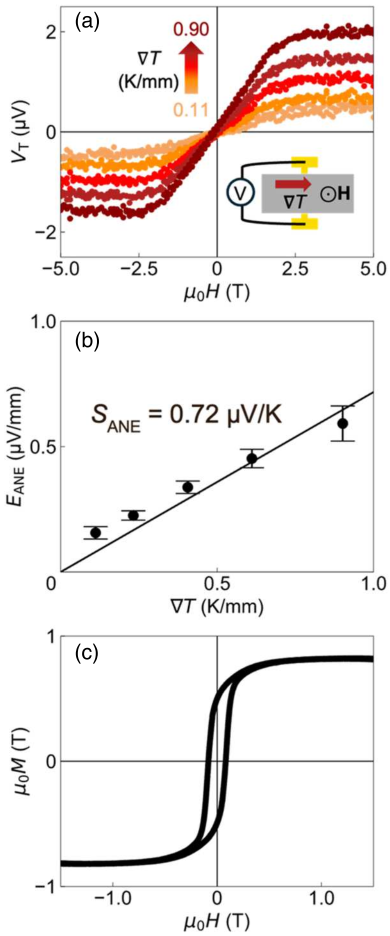

Fig. 3. (a) H dependence of V_T for the $Sm_{19}Co_{81}$ film on a sapphire substrate at various ∇T, measured under an out-of-plane magnetic field. The loop was measured through one measurement for each ∇T. (b) ∇T dependence of E_{ANE}. Each data point was calculated by dividing the average V_T in the range of $|\mu_0 H| = 3$–5 T by the wire width and the error bar represents the standard deviation. The solid line shows the result of linear fitting. (c) H dependence of M, measured under an in-plane magnetic field using a vibrating sample magnetometer. All the measurements were performed at room temperature.

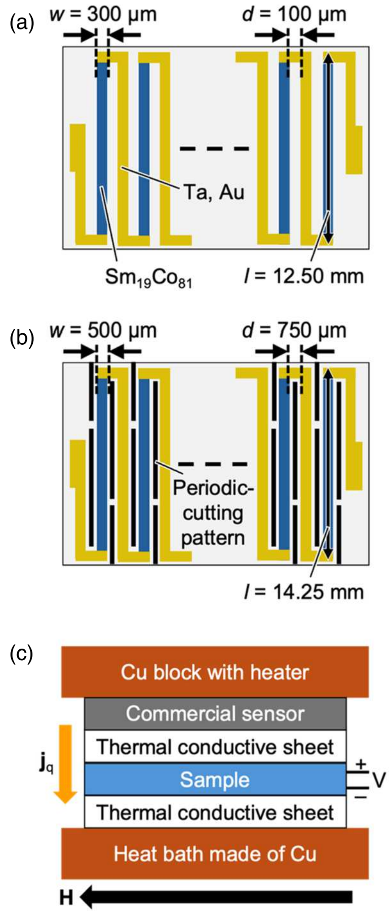

Fig. 4. (a),(b) Blueprints of the thermopile structure consisting of the $Sm_{19}Co_{81}$ and Ta/Au electrode wires on the UPILEX® substrates for the uncut sensor (a) and kirigami-cut sensor (b). In the kirigami-cut sensor, slits with a length of 5.0 and 7.5 mm were arrayed on the gaps between the $Sm_{19}Co_{81}$ and Ta/Au wires. (c) Schematic of the experimental setup to evaluate the heat flux sensitivity of the ANE-based heat flux sensor. Here, the thickness of ANE-based heat flux sensor, Seebeck-effect-based heat flux sensor, and thermal conductive sheet is about 50 μm, 400 μm, and 100 μm, respectively.

average V_T in the range of $|\mu_0 H| = 3$–5 T by the wire width. Figure 3(b) shows the ∇T dependence of E_{ANE}. The S_{ANE} value of our $Sm_{19}Co_{81}$ film was estimated to be 0.72 $\mu V K^{-1}$. This value is comparable but slightly smaller than that reported in previous studies,[5] which may be attributed to differences in sputtering conditions[35] and nanostructure in amorphous films.[36] Although this $Sm_{19}Co_{81}$ film has no perpendicular magnetic anisotropy [Fig. 3(a)], the clear hysteresis loop was observed in the in-plane magnetic field with remanent magnetization and coercivity [Fig. 3(c)]. From these results, heat flux sensing without any external magnetic field is expected by using $Sm_{19}Co_{81}$ as a magnetic material of thermopiles.

Then, we prepared two types of ANE-based heat flux sensors: the sensors without and with a periodic-cutting pattern, referred to as an uncut sensor and kirigami-cut sensor, respectively. The procedure for making the uncut sensor is as follows. After depositing the 100-nm-thick $Sm_{19}Co_{81}$ film on the UPILEX® substrate, the film was processed to multiple wires with the width $w = 300$ μm and length l using photolithography and Ar ion milling. Subsequently, 5-nm-thick Ta and 150-nm-thick Au films were deposited and processed to electrode wires with $w = 300$ μm by the lift-off method [Fig. 4(a)]. The interval between the $Sm_{19}Co_{81}$ and Ta/Au wires d was 100 μm. For making the kirigami-cut sensor, prior to the $Sm_{19}Co_{81}$ film deposition, the kirigami cutting pattern was introduced into the UPILEX® substrate using a CO_2 laser. Then, the $Sm_{19}Co_{81}$ and Ta/Au electrode wires with $w = 500$ μm and $d = 750$ μm were formed in the same manner as the fabrication of the uncut sensor [Fig. 4(b)]. The values of l in the uncut and kirigami-cut sensors were 12.50 and 14.25 mm, respectively. In ANE-based heat flux sensors, the output voltage signal V_{ANE} depends on the total length of the magnetic wire.[37] Thus, to quantitatively compare the performance as the heat flux sensor, the normalized heat flux sensitivity $V_{ANE}/j_q nl$ was estimated, where j_q is the heat flux density and n is the number of the $Sm_{19}Co_{81}$ wire contributing V_{ANE} generation (note that we adopted the asymmetric kirigami structure to increase total length of magnetic wire). For this estimation, the ANE-based heat flux sensor and a 15-mm-square commercially available Seebeck-effect-based heat flux sensor (HF15, Captec Entreprise) were sandwiched by a heater and heat bath, both made of Cu [Fig. 4(c)].[1,5] To improve the thermal contact, thermal conductive sheets (15-mm-square, matching the size of the Seebeck-effect-based heat flux sensor) were inserted at the top and bottom surface of the ANE-based heat flux sensor. The heat flux was applied in the out-of-plane direction through two Cu blocks in an ambient temperature and pressure and in-plane H was swept under thermal equilibrium conditions, allowing the heat flux density j_q, calculated using the calibration function provided by the manufacturer of the Seebeck-effect-based heat flux sensor, and V_{ANE} from the ANE-based heat flux sensor and to be measured simultaneously. The n value associated with the size of the heater was determined using a charge-coupled device camera, yielding 19 (6) for the uncut (kirigami-cut) sensor. We estimated the $V_{ANE}/j_q nl$ values for three configurations: the uncut sensor (Uncut), kirigami-cut sensor without extension (Kirigami without extension), and kirigami-cut sensor with 10% extension of its full length (Kirigami with 10% extension). In the sensitivity evaluation of Kirigami with 10% extension, the kirigami-cut sensor was extended to 10% strain and then clamped between the heater and heat bath to fix the stretched state.

Figures 5(a)–5(c) show the H dependence of V_{ANE}/nl for the samples of Uncut, Kirigami without extension, and Kirigami with 10% extension, respectively. In all measurements, the hysteresis of V_{ANE}/nl was observed although the coercivity was slightly different between the uncut and kirigami-cut sensors. Importantly, both the remanent and saturation V_{ANE}/nl values showed similar values in three configurations. Figures 5(d)–5(f) reveal the proportional relationship between j_q and V_{ANE}/nl both at the remanent ($|\mu_0 H| = 0$ T) and magnetically saturated states ($|\mu_0 H| = 0.3$ T) for three configurations. The solid lines in Figs. 5(d)–5(f) show the results of linear fitting and their slopes indicate $V_{ANE}/j_q nl$. Table I summarizes the $V_{ANE}/j_q nl$ values at $|\mu_0 H| = 0$ and 0.3 T for three configurations. Notably, the $V_{ANE}/j_q nl$ value of the kirigami-cut sensor exhibited no change either without or with extension. It is known that uniform stretching of a kirigami sheet introduces locally non-uniform strain within the patterned region.[23,26,27,30] The invariance of V_{ANE} against such strain distribution indicates that the thermoelectric transport properties of the amorphous $Sm_{19}Co_{81}$ film are insensitive to strain and further suggests robust sensor operation even in the presence of the non-uniform strain inevitably induced by three-dimensional deformation (note that, in the present configuration, out-of-plane deformation of kirigami was suppressed by clamping the sensor between Cu blocks, which resulted in a slight difference in the internal strain distribution from that arising from simple uniaxial stretching). In addition, the invariant V_{ANE}, despite the change in heat transfer area upon the 10% extension–even with the formation of void regions induced by stretching the kirigami–ensures the assumption of one-dimensional heat flow in the kirigami-cut sensor owing to its low thermal resistance [this assumption is reasonable given that the sensors and sheets are very thin (total thickness is about 0.6 mm) relative to the clamping region (about 15 mm square)], thereby enabling the quantitative estimation of j_q under the various deformation conditions.

In summary, we proposed a flexible architecture of ANE-based heat flux sensors by designing a kirigami structure onto the flexible substrate and demonstrated its sensor operation at zero magnetic field. Kirigami structuring did not deteriorate the performance as a heat flux sensor, and the sensor characteristics remained unchanged even under 10% stretching, which is the most basic deformation of kirigami structure, yet far exceeds the elastic limit of uncut flexible substrates (typically a few %[31,38,39]). Since numerous kirigami patterns exist beyond the one employed in this study and provide a wide variety of deformability, optimization of the kirigami structure will further boost the mechanical adaptability of the heat flux sensor comprising magnetic thin films. Specifically, to realize thermoelectric heat flux sensing on arbitrary curved surfaces, it is necessary to optimize both the kirigami design and selection of substrate materials to prevent thermal contact from deteriorating due to out-of-plane deformation of kirigami. Finally, it should be

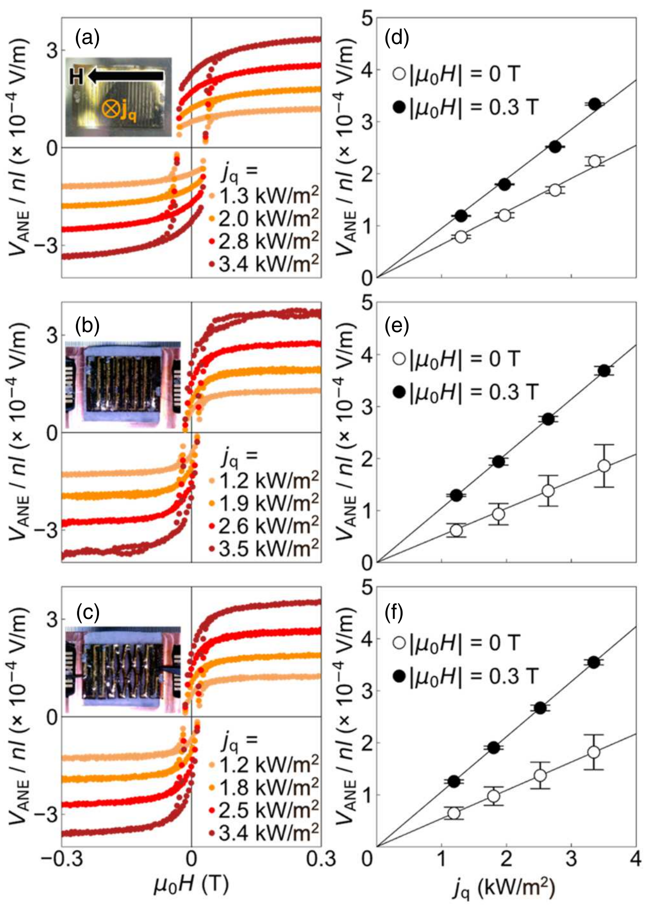

Fig. 5. (a)–(c) H dependence of V_{ANE}/nl for Uncut (a), Kirigami without extension (b), and Kirigami with 10% extension (c) at various values of j_q. The insets show the photograph of the fabricated sensors. The loop at each j_q represents the average of three measurements. (d)–(f) j_q dependence of V_{ANE}/nl extracted at $|\mu_0 H| = 0$ and 0.3 T for Uncut (d), Kirigami without extension (e), and Kirigami with 10% extension (f).

Table I. $V_{ANE}/j_q nl$ value at remanent and magnetically saturated states for the configurations of Uncut, Kirigami without extension, and Kirigami with 10% extension.

	$V_{ANE}/j_q nl$ ($\times 10^{-7}$ VW^{-1}m)		
$|\mu_0 H|$ (T)	Uncut	Kirigami without extension	Kirigami with 10% extension
0	0.62 ± 0.01	0.51 ± 0.05	0.54 ± 0.05
0.3	0.93 ± 0.01	1.05 ± 0.01	1.06 ± 0.01

noted that the device architecture based on kirigami structure proposed in this study can be applied not only to ANE but also to other transverse thermoelectric conversion phenomena,[37] highlighting the versatility of this concept.

Acknowledgments The authors thank D. Chiba for technical support and K. Hirata and Y. Nakanishi for valuable discussions. This work was supported by ERATO "Magnetic Thermal Management Materials Project" (No. JPMJER2201) from JST, Japan; Grant-in-Aid for Early-Career Scientists (No. 25K17940), and Grant-in-Aid for Scientific Research (C) (No. 25K08463) from JSPS KAKENHI, Japan; Resonac Corporation; and NIMS Joint Research Hub Program.

ORCID iDs Takamasa Hirai https://orcid.org/0000-0002-5577-8018 Weinan Zhou https://orcid.org/0000-0003-2946-9913 Shunsuke Mori https://orcid.org/0000-0002-1193-4322 Kota Hasegawa https://orcid.org/0009-0008-3508-1740 Rajkumar Modak https://orcid.org/0000-0001-7939-3289 Fuyuki Ando https://orcid.org/0009-0003-7789-8170 Yuya Sakuraba https://orcid.org/0000-0003-4618-9550 Ken-ichi Uchida https://orcid.org/0000-0001-7680-3051

1) W. Zhou and Y. Sakuraba, Appl. Phys. Express **13**, 043001 (2020).
2) S. Isogami, K. Masuda, Y. Miura, N. Rajamanickam, and Y. Sakuraba, Appl. Phys. Lett. **118**, 092407 (2021).
3) K. Uchida, W. Zhou, and Y. Sakuraba, Appl. Phys. Lett. **118**, 140504 (2021).
4) T. Higo, Y. Li, K. Kondou, D. Qu, M. Ikhlas, R. Uesugi, D. Nishio-Hamane, C. L. Chien, Y. Otani, and S. Nakatsuji, Adv. Funct. Mater. **31**, 2008971 (2021).
5) R. Modak et al., Sci. Technol. Adv. Mater. **23**, 767 (2022).
6) H. Tanaka, T. Higo, R. Uesugi, K. Yamagata, Y. Nakanishi, H. Machinaga, and S. Nakatsuji, Adv. Mater. **35**, 2303416 (2023).
7) H. Imaeda, R. Toida, T. Takeuchi, H. Awano, and K. Tanabe, Appl. Phys. Lett. **125**, 044101 (2024).
8) K. Ito, T. Kubota, and K. Takanashi, Phys. Rev. Appl. **21**, 054012 (2024).
9) S. J. Park, K. M. Bang, J. Park, and H. Jin, Appl. Therm. Eng. **265**, 125555 (2025).
10) S. Noguchi, K. Fujiwara, Y. Yanagi, M. Suzuki, T. Hirai, T. Seki, K. Uchida, and A. Tsukazaki, Nat. Phys. **20**, 254 (2024).
11) Y. Sakuraba, Scr. Mater. **111**, 29 (2016).
12) J. Wang, A. Miura, R. Modak, Y. K. Takahashi, and K. Uchida, Sci. Rep. **11**, 11228 (2021).
13) H. Yuan and Z. Ma, Appl. Phys. Lett. **89**, 212105 (2006).
14) P. Hu et al., Nano Lett. **13**, 1649 (2013).
15) Y. Li, L. Meng, Y. Yang, G. Xu, Z. Hong, Q. Chen, J. You, G. Li, Y. Yang, and Y. Li, Nat. Commun. **7**, 10214 (2016).
16) S. Ota, A. Ando, and D. Chiba, Nat. Electron. **1**, 124 (2018).
17) T. Hirai, H. Sepehri-Amin, K. Hasegawa, T. Koyama, R. Iguchi, T. Ohkubo, D. Chiba, and K. Uchida, Appl. Phys. Lett. **118**, 022403 (2021).
18) M. Hassan, G. Abbas, N. Li, A. Afzal, Z. Haider, S. Ahmed, X. Xu, C. Pan, and Z. Peng, Adv. Mater. Technol. **7**, 2100773 (2022).
19) N. Jang, K. Kim, S. Ha, S. Jung, H. M. Lee, and J. Kim, Appl. Mater. Interfaces **9**, 19612 (2017).
20) R. Zhao, S. Lin, H. Yuk, and X. Zhao, Soft Matter **14**, 2515 (2018).
21) J. Chen, Y. Shi, B. Ying, Y. Hu, Y. Gao, S. Luo, and X. Liu, Mater. Horiz. **11**, 2010 (2024).
22) A. Lamoureux, K. Lee, M. Shlian, S. R. Forrest, and M. Shtein, Nat. Commun. **6**, 8092 (2015).
23) Z. Wang, L. Zhang, S. Duan, H. Jiang, J. Shen, and C. Li, J. Mater. Chem. C **5**, 8714 (2017).
24) Y. Morikawa, S. Yamagiwa, H. Sawahata, R. Numano, K. Koida, M. Ishida, and T. Kawano, Adv. Healthcare Mater. **7**, 1701100 (2018).
25) J. J. Park, P. Won, and S. H. Ko, Int. J. of Precis. Eng. and Manuf.-Green Tech. **6**, 147 (2019).
26) T. Hirai, R. Iguchi, A. Miura, and K. Uchida, Adv. Funct. Mater. **32**, 2201116 (2022).
27) Y. Kim, J. Song, S. Hong, and S. Ahn, npj Flexible Electron. **6**, 52 (2022).
28) T. Kim, H. Moeinnia, and W. S. Kim, Mater. Des. **234**, 112332 (2023).
29) N. Nakamura and E. Iwase, npj Flexible Electron. **9**, 51 (2025).
30) S. Terashima, M. Ohnishi, J. Shiomi, and E. Iwase, npj Flexible Electron. **9**, 105 (2025).
31) S. Ota, A. Ando, T. Sekitani, T. Koyama, and D. Chiba, Appl. Phys. Lett. **115**, 202401 (2019).
32) J. Reslan, O. Kassem, V. Barnier, S. Sao-joao, F. Vacandio, M. Saadaoui, and T. Djenizian, Energy Mater. **5**, 500137 (2025).
33) T. Hirai, F. Ando, H. Sepehri-Amin, and K. Uchida, Nat. Commun. **15**, 9643 (2024).
34) K. Uchida, T. Hirai, F. Ando, and H. Sepehri-Amin, Adv. Energy Mater. **14**, 2302375 (2024).
35) H. Mizuno, R. Modak, T. Hirai, A. Takahagi, Y. Sakuraba, R. Iguchi, and K. Uchida, Appl. Phys. Lett. **120**, 202401 (2022).
36) R. Gautam, T. Hirai, A. Alasli, H. Nagano, T. Ohkubo, K. Uchida, and H. Sepehri-Amin, Nat. Commun. **15**, 2184 (2024).
37) H. Adachi, F. Ando, T. Hirai, R. Modak, M. A. Grayson, and K. Uchida, Appl. Phys. Express **18**, 090101 (2025).
38) T. Uhrmann, L. Bär, T. Dimopoulos, N. Wiese, M. Rührig, and A. Lechner, J. Magn. Magn. Mater. **307**, 209 (2006).
39) J. Sun, N. Lu, J. Yoon, K. Oh, Z. Suo, and J. J. Vlassak, J. Mater. Res. **24**, 3338 (2009).